

This is the accepted manuscript made available via CHORUS. The article has been published as:

^{57}Fe Mössbauer study of magnetic ordering in
superconducting $\text{K}_{0.80}\text{Fe}_{1.76}\text{Se}_{2.00}$ single
crystals

D. H. Ryan, W. N. Rowan-Weetaluktuk, J. M. Cadogan, R. Hu, W. E. Straszheim, S. L.
Bud'ko, and P. C. Canfield

Phys. Rev. B **83**, 104526 — Published 31 March 2011

DOI: [10.1103/PhysRevB.83.104526](https://doi.org/10.1103/PhysRevB.83.104526)

^{57}Fe Mössbauer study of magnetic ordering in superconducting $\text{K}_{0.80}\text{Fe}_{1.76}\text{Se}_{2.00}$ single crystals

D.H. Ryan,¹ W.N. Rowan-Weetaluktuk,¹ J.M. Cadogan,² R. Hu,³ W.E. Straszheim,³ S.L. Bud'ko,³ and P.C. Canfield³

¹*Physics Department and Centre for the Physics of Materials,
McGill University, Montreal, H3A 2T8, Canada*

²*Department of Physics and Astronomy, University of Manitoba, Winnipeg, Manitoba, R3T 2N2, Canada*

³*Ames Laboratory, U.S. DOE and Department of Physics and Astronomy, Iowa State University, Ames, IA 50011, USA*

(Dated: March 29, 2011)

The magnetic ordering of superconducting single crystals of $\text{K}_{0.80}\text{Fe}_{1.76}\text{Se}_{2.00}$ has been studied between 10 K and 550 K using ^{57}Fe Mössbauer spectroscopy. Despite being superconducting below $T_{sc} \sim 30$ K, the iron sublattice in $\text{K}_{0.80}\text{Fe}_{1.76}\text{Se}_{2.00}$ clearly exhibits magnetic order from well below T_{sc} to its Néel temperature of $T_N = 532 \pm 2$ K. The iron moments are ordered almost parallel to the crystal c -axis. The order collapses rapidly above 500 K and the accompanying growth of a paramagnetic component suggests that the magnetic transition may be first order, which may explain the unusual temperature dependence reported in recent neutron diffraction studies.

PACS numbers:

I. INTRODUCTION

The co-existence of magnetism and superconductivity in the new iron-chalcogenide superconductors raises the possibility of unconventional pairing mechanisms that may be associated with their magnetism.¹⁻⁴ As with the more established cuprate superconductors, the iron-based superconductors have layered structures; the planar Fe layers tetrahedrally coordinated by As or chalcogen anions (Se or Te) are believed to be responsible for superconductivity. Stacking of the FeAs building blocks with alkali, alkaline earth or rare earth-oxygen spacer layers forms the basic classes of iron arsenic superconductors in these compounds: 111-type AFeAs ⁵, 122-type AFe_2As_2 ⁶⁻⁹, 1111-type ROFeAs ^{10,11} and more complex block containing phases, e.g. $\text{Sr}_2\text{VO}_3\text{FeAs}$ ¹², $\text{Sr}_3\text{Sc}_2\text{Fe}_2\text{As}_2\text{O}_5$ ¹³, $\text{Sr}_4\text{Sc}_2\text{Fe}_2\text{As}_2\text{O}_6$ ¹⁴. The simple binary 11-type iron chalcogenides have no spacer layers and superconductivity can be induced by doping FeTe with S¹⁵ or Se¹⁶. Unlike the other iron-based superconductors, FeSe is a superconductor¹⁷, $T_{sc} \sim 8$ K, with no static magnetic order and its transition temperature can be increased up to 37 K by applying pressure¹⁸ or 15 K in $\text{FeSe}_{0.5}\text{Te}_{0.5}$ ¹⁶. More recently, superconductivity above 30 K has been reported in $\text{A}_x\text{Fe}_{2-y}\text{Se}_2$ ($\text{A} = \text{K}, \text{Cs}, \text{Rb}$ or Tl)¹⁹⁻²³, a compound with the same unit cell structure as the AFe_2As_2 compounds.

μSR measurements showed that magnetic order co-exists with bulk superconductivity in $\text{Cs}_{0.8}\text{Fe}_{1.6}\text{Se}_2$ ²⁴, while neutron diffraction measurements on $\text{K}_{0.8}\text{Fe}_{1.6}\text{Se}_2$ ²⁵ have suggested that not only do magnetic order and superconductivity co-exist, but that the iron moments are remarkably large ($3.31 \mu_B/\text{Fe}$) and are ordered in a relatively complex antiferromagnetic structure that places all of the iron moments parallel to the c -axis. The magnetic ordering temperatures are quite high in both compounds: $T_N(\text{Cs})=480$ K²⁴, $T_N(\text{K})=560$ K²⁵. The development of a paramagnetic component near T_N ²⁴ and the unusual temperature

dependence of the magnetic intensity²⁵ suggest that the magnetic transition may be first order in nature rather than being a more conventional second order transition. First order magnetic transitions are commonly associated with changes in crystal structure, and both synchrotron x-ray diffraction²⁶ and neutron diffraction^{25,27} have now shown evidence for a structural change from $I4/m$ to $I4/mmm$ associated with a disordering of iron vacancies that occurs in the vicinity of the magnetic transition. However, the magnetic structure adopted by the iron sublattice has not been confirmed, and room temperature neutron diffraction studies of $\text{Cs}_y\text{Fe}_{2-x}\text{Se}_2$ ²⁶ and $\text{A}_y\text{Fe}_{2-x}\text{Se}_2$ ($\text{A} = \text{Rb}, \text{K}$)²⁸ have suggested that the iron moments may be much smaller ($\sim 2.5 \mu_B/\text{Fe}$) and also that the magnetic structure may be far more complex than initially suggested, with the iron atoms being distributed among two (magnetically) inequivalent sublattices and carrying very different magnetic moments. Moreover, even the ordering *direction* has been questioned and it is possible that the iron moments may lie in the ab -plane, at least for $\text{Cs}_y\text{Fe}_{2-x}\text{Se}_2$ ²⁶, rather than parallel to the c -axis as initially suggested²⁵.

Given the many questions surrounding the magnetic ordering of the iron moments in the $\text{A}_y\text{Fe}_{2-x}\text{Se}_2$ system, we have undertaken a ^{57}Fe Mössbauer study $\text{K}_{0.80}\text{Fe}_{1.76}\text{Se}_{2.00}$. While Mössbauer spectroscopy cannot be used to determine magnetic structures directly, it is a quantitative local probe that can be used to set hard limits on possible structures. As we will show below, the observation of a single, well-split magnetic component allows us to rule out any structure in which the iron sublattice is further subdivided into multiple, inequivalent sites, and the scale of the splitting (~ 29 T at 10 K) is consistent with the $3.31 \mu_B$ moment derived from neutron scattering²⁵. Furthermore, by working with single crystal samples, we are able to demonstrate that the moments order parallel to the c -axis, ruling out any models that invoke planar ordering. Finally, the development of

a paramagnetic component that co-exists with the magnetically ordered phase and that grows at its expense on heating through T_N , confirms that the magnetic transition is indeed first order in nature.

II. EXPERIMENTAL METHODS

The preparation and characterisation of the crystals used in this study has been described in detail elsewhere²³ so only a basic description will be provided here. Single crystals of $K_{0.8}Fe_{1.76}Se_{2.00}$ were grown from a $K_{0.8}Fe_2Se_2$ melt, as described in Ref.²⁰. First the FeSe precursor was prepared by reacting stoichiometric Fe and Se at 1050°C. Then, K and FeSe with a nominal composition of $K_{0.8}Fe_2Se_2$ were placed in an alumina crucible that was sealed in an amorphous silica tube. The growth was placed in a furnace in a vented enclosure and heated to 1050°C, where it was held for a 2 hour soak. The furnace temperature was then slowly lowered to 750°C over 50 hours; the furnace was then turned off and the sample “furnace cooled” over an additional 10 hours. Once the ampoules were opened, large ($\sim 1 \times 1 \times 0.02$ cm³) dark shiny crystals could be mechanically separated from the solidified melt.

Crystals were characterised by powder x-ray diffraction using a Rigaku Miniflex X-ray diffractometer. The average chemical composition was determined by examining multiple points on a cleaved surface of the crystal, using wavelength dispersive x-ray spectroscopy (WDS) in a JEOL JXA-8200 electron microscope. A backscattered electron analysis (BSE) was performed using an accelerating voltage of 20 kV. Magnetic susceptibility was measured in a Quantum Design MPMS, SQUID magnetometer. The x-ray diffraction pattern can be indexed using the I4/mmm space group, with lattice parameters refined by Rietica of $a = 3.8897(8)\text{\AA}$ and $c = 14.141(3)\text{\AA}$, in good agreement with previous values²⁰. The in-plane resistivity of the furnace cooled sample is very similar to that of earlier reports^{20,29}: a broad resistive maximum centered near 160 K is followed by a drop of nearly a factor of 6 (ρ_{300K}/ρ_{35K}). The sharp transition to zero resistance gives an onset temperature of $T_{sc} = 30.1$ K. Corresponding features were also seen in the susceptibility and heat capacity.

The as-grown crystals were too thick to serve as Mössbauer absorber but we found that they could be cleaved quite easily using a razor blade, much like mica, and many large-area plates could be formed from each crystal. Two single crystal mosaic samples were prepared from the same batch of crystals. The first, for low-temperature work, was prepared by attaching several single crystal plates to a 12 mm diameter disc of 100 μ m thick Kapton foil using Apiezon N grease. Care was taken to ensure that there were no gaps, but minimal overlap between the crystals. This sample was transferred promptly to a vibration-isolated closed-cycle refrigerator with the sample held in vacuum. The second

sample, for the high-temperature work, was attached to a $\frac{1}{2}$ -inch diameter 10-mil beryllium disc using diluted GE-7031 varnish before being mounted in a resistively heated oven, again with the sample in vacuum. While we operated somewhat above the maximum service temperature of the varnish, the sample was cycled above 250°C three times without any evidence of degradation.

The Mössbauer spectra were collected on conventional spectrometers using 50 mCi ⁵⁷CoRh sources mounted on electromechanical drives operated in constant acceleration mode (on the high-temperature system) and sine-mode (on the low-temperature system). The spectrometers were calibrated against α -Fe metal at room temperature. The closed-cycle refrigerator cools to 10 K, with temperature sensing and control using a calibrated silicon diode mounted on the copper sample stage. Measured gradients (centre to edge of sample) in the oven are less than 1 K up to 750 K. Control and sensing rely on four type-K thermocouples. Temperature stability in both cases is better than 0.2 K. Spectra were fitted using a conventional non-linear least-squares minimisation routine to a sum of equal-width Lorentzian lines. Magnetic patterns were fitted assuming first-order perturbation in order to combine the effects of the magnetic hyperfine field (B_{hf}) and the electric field gradient.

III. RESULTS

Several conclusions can be reached simply by inspection of the spectrum taken at 10 K (Fig. 1). The spectrum is dominated by a single, well-split, magnetic component. This confirms that $K_{0.8}Fe_{1.76}Se_{2.00}$ is indeed magnetically ordered in the superconducting state (recall $T_{sc} \sim 30$ K for this sample). A small quadrupole splitting of 0.33 ± 0.02 mm/s is present and the linewidth (full width at half maximum) is 0.200 ± 0.007 mm/s, slightly larger than our typical instrumental width of 0.15 mm/s. The single magnetic component allows us to rule out any magnetic structures involving multiple iron sub-sites with moments that differ by more than a few percent. As we will show below, the large hyperfine field ($B_{hf} \sim 29$ T) is inconsistent with a small iron moment and so places further limits on possible magnetic structures. Finally, two of the lines normally present in a magnetically split ⁵⁷Fe Mössbauer spectra, are essentially absent from the 10 K pattern.

A magnetic field at the ⁵⁷Fe nucleus, either externally applied or transferred from an ordered moment on the iron atom, lifts the degeneracy of the nuclear states and, in combination with the selection rules for the $\frac{3}{2} \rightarrow \frac{1}{2}$ transition, leads to a six-line pattern with intensities of 3:R:1:1:R:3 (counting from left to right in Fig. 1). For a powder sample, R=2, however if there is a unique angle, θ , between the magnetic field and the direction of the γ -beam used to record the spectrum, then the intensity,

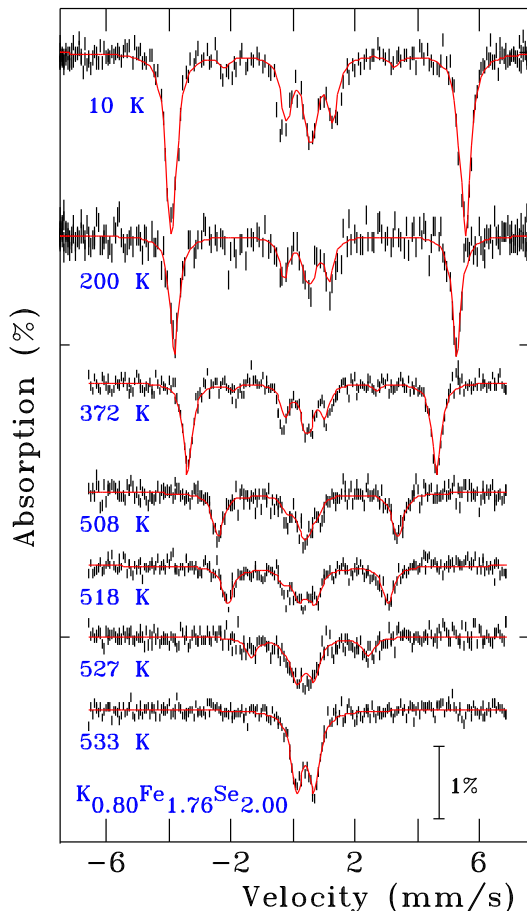


FIG. 1: (color online) ^{57}Fe Mössbauer spectra of $\text{K}_{0.80}\text{Fe}_{1.76}\text{Se}_{2.00}$ showing the evolution of the magnetic ordering on heating from 10 K (well below $T_{sc} \sim 30$ K) to 533 K where the material is paramagnetic. The extreme weakness of the $\Delta m_I = 0$ transitions in the ordered state indicates that the moments are almost parallel to the crystal c -axis (see text), while the growth of a central paramagnetic component above 500 K is characteristic of a first order magnetic transition. Solid lines are fits as described in the text.

R , of the $\Delta m_I = 0$ transitions is given by:

$$R = \frac{4 \sin^2 \theta}{1 + \cos^2 \theta}$$

$R=0$ implies that θ is also zero so that the magnetic field, and by extension, the moments that lead to it, is parallel to the γ -beam. Since the sample consists of an ab-plane mosaic of single crystals, setting $\theta = 0$ means that the magnetic ordering direction is parallel to the c -axis, ruling out any magnetic structures that involve planar ordering of the iron moments. We note that R is a relatively soft function of θ near zero, and a free fit to the intensity of the $\Delta m_I = 0$ transitions is consistent with an angle of $18 \pm 4^\circ$, and leads to a slight improvement in χ^2 for the fit. Such an angle would not be consistent with a purely planar ordering of the iron moments (indeed, if the ordering were planar, then R would be 4, and the

$\Delta m_I = 0$ transitions would provide the strongest features in the spectrum) but it is too large to be dismissed as being due to a simple mis-alignment of the mosaic. This suggests that there is a small canting of the antiferromagnetic structure away from the c -axis.

Estimating the iron moment from the observed hyperfine field requires some care as the scaling is imperfect at best³⁰. However, some data exist on binary iron-chalcogenides that can be used as a guide (Table I). If we use the factor of $6.2 \text{ T}/\mu_B$ for Fe_7Se_8 with our measured B_{hf} of 29.4 T we obtain a rather large estimate of $4.7 \mu_B/\text{Fe}$ for the iron moment in this system. This is significantly larger than the $3.31 \mu_B/\text{Fe}$ reported on the basis of neutron diffraction²⁵, however it does suggest that the iron moment is indeed substantial as even the larger conversion factor for the sulphide yields $3.5 \mu_B/\text{Fe}$. If we assume that B_{hf} is at least proportional to the iron moment, then we can use the observed change in B_{hf} between 10 K and 293 K to scale the $3.31 \mu_B/\text{Fe}$ observed at 11 K²⁵ to get an estimate of $3.0 \mu_B/\text{Fe}$ for the moment at room temperature for comparison with the much smaller value of $2.55 \mu_B/\text{Fe}$ reported by Pomjakushin *et al.*²⁸. However, the strong temperature dependence of magnetic signal noted by Bao *et al.*²⁵ suggests a very rapid decline in ordered moment to about $2.8 \mu_B/\text{Fe}$ by room temperature. It is possible that much of the variation may be intrinsic to the material and its variable stoichiometry, so that combined measurements on a well characterised sample will be needed to settle this.

Impurities may provide a possible origin for the variation in measured moments. Mössbauer spectroscopy, while sensitive to the presence of impurity phases, does not rely on normalisation to the total sample in order to determine moments, they come rather from the observed line splitting, and not the intensity. Neutron diffraction, by contrast, while providing far more information on the magnetic ordering, ultimately relies on peak intensities, normalised to the total nuclear scattering, to determine the magnetic moments. It is clear from the 10 K spectrum shown in Fig. 1 that there is a central paramagnetic component present that involves about $12 \pm 2\%$ of the iron in the sample. Such high apparent impurity levels in single crystal samples with no impurities detected by powder x-ray diffraction²³, deserves further attention. If the paramagnetic component is not an “impurity” then it must either be intrinsic to the structure or a property of the material.

At the temperatures of interest here, $\text{K}_{0.80}\text{Fe}_{1.76}\text{Se}_{2.00}$ adopts a vacancy-ordered $I4/m$ modification of the parent ThCr_2Si_2 -type $I4/mmm$ structure with iron essentially filling a $16i$ site and leaving ordered vacancies on the (almost) empty $4d$ site^{26,31}. Occupations of $\sim 8\%$ for the Fe- $4d$ site have been reported³¹. If we assume full occupation of the Fe- $16i$ site in our sample, this leaves 9% of the iron in the $4d$ site. Partial occupation of the Fe- $16i$ site would leave more iron to be accommodated in the $4d$ site. As we see no evidence for a second magnetic component that could be associated with iron in the $4d$

TABLE I: Average hyperfine fields (B_{hf}) derived from ^{57}Fe Mössbauer spectroscopy and average iron moments derived from neutron diffraction for approximately equi-atomic iron-chalcogenide compounds with estimated field-moment conversion factors. The Fe-Te system exhibits significant variability and measurements have yet to be made on common samples making the conversion factor unreliable. There is however a clear trend to lower values in the sequence $\text{S} \rightarrow \text{Se} \rightarrow \text{Te}$.

Compound	Average B_{hf} (T)	Average moment μ_B/Fe	Conversion Factor T/μ_B
Sulphides			
Fe_7S_8	26.8 ³²	3.16 ³³	8.5
Selenides			
Fe_7Se_8	24.1 ³⁴	3.86 ³⁵	6.2
Tellurides			
$\text{Fe}_{1.125}\text{Te}$	—	2.07 ³⁶	
Fe_{1+x}Te $0.076 \leq x \leq 0.141$	—	1.96–2.03 ³⁷	
$\text{Fe}_{1.068}\text{Te}$	—	2.25 ³⁸	
$\text{Fe}_{1.05}\text{Te}$	—	2.54 ³⁹	
$\text{Fe}_{1.11}\text{Te}$	11 ⁴⁰	—	
$\text{Fe}_{1.08}\text{Te}$	10.34 ⁴¹	—	4.3–5.2

site, it is possible that the iron in these more isolated sites does not order, in which case our estimate of $\approx 9\%$ in the 4d site is fully consistent with the $12 \pm 2\%$ paramagnetic component observed in the Mössbauer spectrum.

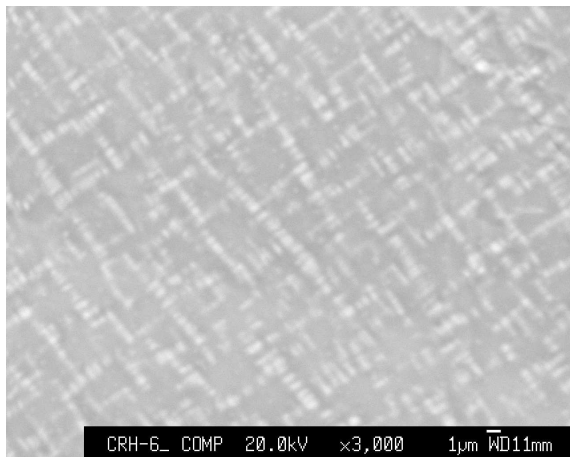


FIG. 2: Backscattered electron analysis (BSE) image of a cleaved crystal surface of $\text{K}_{0.80}\text{Fe}_{1.76}\text{Se}_{2.00}$ taken at an accelerating voltage of 20 kV. The lighter regions have lower potassium concentrations than the darker background area.

Another possible origin of the $12 \pm 2\%$ non-magnetic Fe component in the low temperature (including room tem-

perature) state can be seen in the backscattered electron analysis (BSE) image shown in Fig. 2. This image reveals that there is, at the micron scale, a modulation in the surface composition that can be correlated, through a preliminary line-scan analysis of the WDS data, with reductions of K content in the lighter regions. Given the length scale associated with these regions, combined with the probing volume of the WDS analysis, it is not clear whether this spatial variation is only associated with the surface or is representative of the bulk behaviour of the sample. It should be noted, though, that such patterns appear in samples grown by furnace cooling as well as samples decanted from a liquid melt²³. Regardless of its origin, the non-magnetic Fe signal represents a minority of the Fe sites and does not substantially change with temperature until the first order phase transition is reached.

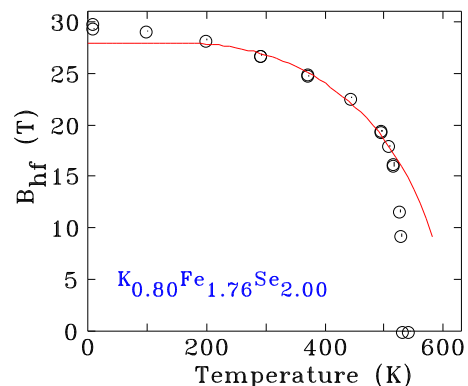


FIG. 3: (color online) Temperature dependence of the magnetic hyperfine field (B_{hf}) in $\text{K}_{0.80}\text{Fe}_{1.76}\text{Se}_{2.00}$. The solid line is a fit to a $J=\frac{1}{2}$ Brillouin function between 200 K and 500 K that yields an expected transition of 600 ± 30 K, well above the observed value of 532 ± 2 K. Fitted errors on B_{hf} are less than 0.1 T, much smaller than the plotting symbols. The rapid collapse above 500 K is accompanied by the growth of a paramagnetic component (see Fig. 4).

Raising the temperature leads to the expected decline in B_{hf} , however it is clear from Fig. 1 that magnetic order persists up to 530 K, confirming that $\text{K}_{0.80}\text{Fe}_{1.76}\text{Se}_{2.00}$ has a remarkably high ordering temperature. The temperature dependence of B_{hf} shown in Fig. 3 yields an ordering temperature of $T_N = 532 \pm 2$ K. However this is not the result of the fit to a $J=\frac{1}{2}$ Brillouin function shown in Fig. 3 as this predicts a transition temperature of 600 ± 30 K and the observed behaviour departs from this curve above 500 K. The two points that bracket the transition are at 530 K, where a clear magnetic signal is seen, and at 533 K where the sample is no longer magnetic, setting the transition at 532 ± 2 K.

A neutron diffraction study of $\text{K}_{0.8}\text{Fe}_{1.6}\text{Se}_2$ found two regions in which the temperature dependence of the magnetic parameter was unusual²⁵. From 50 K to 450 K they found a linear dependence of the (101) magnetic peak intensity, suggesting that μ_{Fe}^2 is a linear function

of temperature. The clear curvature of $B_{hf}(T)$ in this region, shown in Fig. 3, is not consistent with this form, as squaring our observed $B_{hf}(T)$ to get something that would scale with the scattering intensity in a neutron diffraction pattern leads to *increased* curvature rather than linear behaviour.

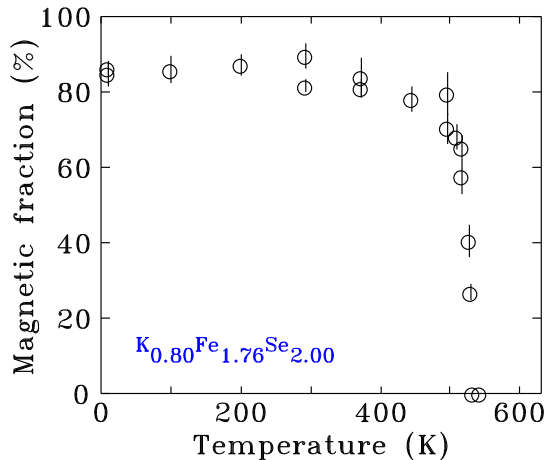


FIG. 4: (color online) Temperature dependence of the magnetic fraction in $K_{0.80}Fe_{1.76}Se_{2.00}$. The rapid collapse above 500 K indicates that the magnetic transition has first order character and may be associated with a structural transition.

Above 500 K, Wei Bao *et al.* reported a very rapid decrease in the (101) intensity²⁵ leading to an ordering temperature of ~ 560 K. While our sample composition is slightly different and our ordering temperature slightly lower, we see the *same* abrupt loss of magnetic order in Fig. 3. Inspection of the spectra above 500 K shown in Fig. 1 reveals that the intensity of the magnetic peaks decreases visibly as their splitting falls. The ability to uniquely separate the amount of a magnetic phase (seen through line intensities) from the magnitude of the magnetic order (seen independently through line splittings) is an important strength of Mössbauer spectroscopy. Tracking the fraction of the iron that is present as a magnetically ordered form (Fig. 4) confirms that the magnetic phase is disappearing even faster than the splitting that marks the order. This strongly suggests that the magnetic phase is transforming before it reaches its true ordering temperature (which we estimate to be about 600 K) and that the observed transition is being driven by a first order structural event. This view is supported by the neutron diffraction work of Wei Bao *et al.*²⁵ where they also tracked the intensity of the (110) structural peak that is associated with the $I4/m$ vacancy-

ordered structure of $K_{0.8}Fe_{1.6}Se_2$ below 580 K. This peak starts to lose intensity at the same temperature at which the (101) magnetic peak starts its sudden decline. As we see both a weakening of the magnetic order and a reduction in the magnetic fraction above 500 K, it is possible that the break-up of the vacancy-ordered magnetic form reduces the magnetic connectivity of the ordered phase until it forms a non-percolating network of finite clusters. The magnetic order is then lost at a temperature below both its intrinsic ordering temperature, and the temperature at which the vacancy-ordered $I4/m$ structure fully transforms to the high-temperature $I4/mmm$ form.

IV. CONCLUSIONS

Our ^{57}Fe Mössbauer spectroscopy study of single crystals of $K_{0.80}Fe_{1.76}Se_{2.00}$ confirms the presence of magnetic order from well below $T_{sc} \sim 30$ K to $T_N = 532 \pm 2$ K. The large magnetic splitting of 29.4 ± 0.1 T at 10 K indicates that the iron moments are large, consistent with values of $3.31 \mu_B/Fe$ observed by neutron diffraction at 11 K²⁵, while the line intensities indicate that the ordering is almost parallel to the c-axis. An apparent paramagnetic impurity phase is attributed to iron atoms in the 4d site. Analysis of the spectra taken in the vicinity of T_N shows that the magnetic fraction decreases rapidly above 500 K and that the loss of order is driven by a first order structural transition as the material transforms into the high-temperature $I4/mmm$ form.

Acknowledgements

Financial support for various stages of this work was provided by the Natural Sciences and Engineering Research Council of Canada and Fonds Québécois de la Recherche sur la Nature et les Technologies. JMC acknowledges support from the Canada Research Chairs programme. R.H. and P.C.C. are supported by AFOSR-MURI grant #FA9550-09-1-0603. W.E.S. and S.L.B. are supported by the U.S. Department of Energy, Office of Basic Energy Science, Division of Materials Sciences and Engineering. Synthesis and basic characterization were performed in Ames Laboratory which is operated for the U.S. Department of Energy by Iowa State University under Contract No. DE-AC02-07CH11358.

¹ Kenji Ishida, Yusuke Nakai, and Hideo Hosono, J. Phys. Soc. Jpn., 78 062001 (2009).

² M. D. Lumsden and A. D. Christianson, J. Phys.: Condens. Matter, 22 203203 (2010).

³ Paul C. Canfield and Sergey L. Bud'ko, Annual Review of Condensed Matter Physics, 1, 27 (2010).

⁴ Johnpierre Paglione and Richard L. Greene, Nature Physics 6, 645 (2010).

- ⁵ X. C. Wang, Q. Q. Liu, Y. X. Lv, W. B. Gao, L. X. Yang, R. C. Yu, F. Y. Li, C. Q. Jin, *Solid State Commun.* **148**, 538 (2008).
- ⁶ M. Rotter, M. Tegel, and D. Johrendt, *Phys. Rev. Lett.* **101**, 107006 (2008).
- ⁷ Athena S. Sefat, Rongying Jin, Michael A. McGuire, Brian C. Sales, David J. Singh, and David Mandrus, *Phys. Rev. Lett.* **101**, 117004 (2008).
- ⁸ N. Ni, M. E. Tillman, J.-Q. Yan, A. Kracher, S. T. Hannahs, S. L. Bud'ko, and P. C. Canfield, *Phys. Rev. B* **78**, 214515 (2008).
- ⁹ A. Leithe-Jasper, W. Schnelle, C. Geibel, and H. Rosner, *Phys. Rev. Lett.* **101**, 207004 (2008).
- ¹⁰ Y. Kamihara, T. Watanabe, M. Hirano, and H. Hosono, *J. Am. Chem. Soc.* **130**, 3296 (2008).
- ¹¹ X. H. Chen, T. Wu, G. Wu, R. H. Liu, H. Chen, and D. F. Fang, *Nature* **453**, 761 (2008).
- ¹² X. Zhu, F. Han, G. Mu, P. Cheng, B. Shen, B. Zeng, and H. H. Wen, *Phys. Rev. B* **79**, 220512 (2009).
- ¹³ X. Zhu, F. Han, G. Mu, B. Zeng, P. Cheng, B. Shen, H. H. Wen, *Phys. Rev. B* **79** 024516 (2009).
- ¹⁴ G. F. Chen, T. L. Xia, H. X. Yang, J. Q. Li, P. Zheng, J. L. Luo, N. L. Wang, *Supercond. Sci. Tech.* **22**, 072001 (2009).
- ¹⁵ Rongwei Hu, Emil S. Bozin, J. B. Warren, and C. Petrovic, *Phys. Rev. B* **80**, 214514 (2009).
- ¹⁶ Y. Mizuguchi, Y. Hara, K. Deguchi, S. Tsuda, T. Yamaguchi, K. Takeda, H. Kotegawa, H. Tou and, Y. Takano, *Supercond. Sci. Tech.*, **23** 054013 (2010).
- ¹⁷ F. C. Hsu, J. Y. Luo, K. W. The, T. K. Chen, T. W. Huang, P. M. Wu, Y. C. Lee, Y. L. Huang, Y. Y. Chu, D. C. Yan and M. K. Wu, *Proc. Nat. Acad. Sci.* **105**, 14262 (2008).
- ¹⁸ S. Medvedev, T. M. McQueen, I. Trojan, T. Palasyuk, M. I. Erements, R. J. Cava, S. Naghavi, F. Casper, V. Ksenofontov, G. Wortmann and C. Felser, *Nature Mater.*, **8** 630 (2009).
- ¹⁹ Jiangang Guo, Shifeng Jin, Gang Wang, Shunchong Wang, Kaixing Zhu, Tingting Zhou, Meng He and Xiaolong Chen, *Phys. Rev. B* **82**, 180520 (2010).
- ²⁰ J. J. Ying, X. F. Wang, X. G. Luo, A. F. Wang, M. Zhang, Y. J. Yan, Z. J. Xiang, R. H. Liu, P. Cheng, G. J. Ye, X. H. Chen, arXiv:1012.5552v1 (2010).
- ²¹ Chun-Hong Li, Bing Shen, Fei Han, Xiyu Zhu, Hai-Hu Wen, arXiv:1012.5637v2 (2010).
- ²² Minghu Fang, Hangdong Wang, Chiheng Dong, Zujuan Li, Chunmu Feng, Jian Chen, H. Q. Yuan, arXiv:1012.5236 (2010).
- ²³ R. Hu, K. Cho, H. Kim, H. Hodovanets, W. E. Straszheim, M. A. Tanatar, R. Prozorov, S. L. Bud'ko, P. C. Canfield, arXiv:1102.1931 (2011).
- ²⁴ Z. Shermadini, A. Krzton-Maziopa, M. Bendele, R. Khasanov, H. Luetkens, K. Conder, E. Pomjakushina, S. Weyeneth, V. Pomjakushin, O. Bossen, A. Amato, arXiv:1101.1873v1 (2011).
- ²⁵ Wei Bao, Q. Huang, G. F. Chen, M. A. Green, D. M. Wang, J. B. He, X. Q. Wang, Y. Qiu, arXiv:1102.0830 (2011).
- ²⁶ V. Yu. Pomjakushin, D. V. Sheptyakov, E. V. Pomjakushina, A. Krzton-Maziopa, K. Conder, D. Chernyshov, V. Svitlyk, Z. Shermadini arXiv:1101.1919 (2011).
- ²⁷ Wei Bao, G. N. Li, Q. Huang, G. F. Chen, J. B. He, M. A. Green, Y. Qiu, D. M. Wang, J. L. Luo, arXiv:1101.3674 (2011).
- ²⁸ V. Yu. Pomjakushin, E. V. Pomjakushina, A. Krzton-Maziopa, K. Conder, Z. Shermadini, arXiv:1101.3380 (2011).
- ²⁹ D. M. Wang, J. B. He, T.-L. Xia, G. F. Chen, arXiv:1101.0789v1 (2011).
- ³⁰ S.M. Dubiel, *J. Alloys Compounds* **488**, 18 (2010).
- ³¹ P. Zavalij, W. Bao, X.F. Wang, J.J. Ying, X.H. Chen, D.M. Wang, J.B. He, X.Q. Wang, G.F. Chen, P-Y Hsieh, Q. Huang, M.A. Green, arXiv:1101.4882 (2011).
- ³² H. Kobayashi, M. Sato, T. Kamimura, M. Sakai, H. Onodera, N. Kuroda and Y. Yamaguchi, *J. Phys.: Condens. Matter*, **9**, 515 (1997).
- ³³ A.V. Powell, P. Vaqueiro, K.S. Knight, L.C. Chapon, and R.D. Sánchez, *Phys. Rev. B* **70**, 014415 (2004).
- ³⁴ H.N. Ok and S.W. Lee, *Phys. Rev. B* **8**, 4267 (1973).
- ³⁵ A.F. Andresen and J. Leciejewicz, *J. de Phys.* **25**, 574 (1964).
- ³⁶ D. Fruchart, P. Convert, P. Wolfers, R. Madar, J.P. Senateur and R. Fruchart, *Mater. Res. Bull.* **10**, 169 (1975).
- ³⁷ Wei Bao, Y. Qiu, Q. Huang, M.A. Green, P. Zajdel, M.R. Fitzsimmons, M. Zhernenkov, S. Chang, M. Fang, B. Qian, E.K. Vehstedt, J. Yang, H.M. Pham, L. Spinu, and Z.Q. Mao, *Phys. Rev. Lett.* **102**, 247001 (2009).
- ³⁸ S. Li, C. de la Cruz, Q. Huang, Y. Chen, J.W. Lynn, J. Hu, Y.-L. Huang, F.-C. Hsu, K.-W. Yeh, M.-K. Wu, and P. Dai, *Phys. Rev. B* **79**, 054503 (2009).
- ³⁹ A. Martinelli, A. Palenzona, M. Tropeano, C. Ferdeghini, M. Putti, M.R. Cimberle, T.D. Nguyen, M. Affronte, and C. Ritter, *Phys. Rev. B* **81**, 094115 (2010).
- ⁴⁰ E. Hermon, W.B. Muir, J. Quaroni, and R.C. Sweet, *Can. J. Phys.* **52**, 1800 (1974).
- ⁴¹ Y. Mizuguchi, T. Furubayashi, K. Deguchi, S. Tsuda, T. Yamaguchi, Y. Takano, *Physica C* **470**, S338 (2010).